Nuclear Instruments and Methods in Physics Research A 623 (2010) 895–902

Contents lists available at ScienceDirect

Nuclear Instruments and Methods in Physics Research A

journal homepage: www.elsevier.com/locate/nima

High power input coupler development for BEPCII 500 MHz superconducting cavity

Tongming Huang [a,*], Weimin Pan [a], Qiang Ma [a], Guangwei Wang [a], Xuwen Dai [a], Zhanjun Zhang [a], T. Furuya [b], S. Mitsunobu [b]

[a] Institute of High Energy Physics, Chinese Academy of Sciences, Beijing 100049, China
[b] KEK, Tsukuba-shi 305-0801, Japan

ARTICLE INFO

Article history:
Received 20 July 2010
Received in revised form
21 August 2010
Accepted 27 August 2010
Available online 7 September 2010

Keywords:
High power input coupler
Superconducting cavity
High power conditioning

ABSTRACT

A high power input coupler for a 500 MHz superconducting cavity (SCC) of the upgrade project of Beijing Electron Positron Collider (BEPCII) has been developed in China. Several prototypes have been fabricated and tested successfully. A maximum of 420 kW continuous wave (CW) RF power in traveling wave (TW) mode was achieved in the high power test. The detailed design, fabrication and test of the coupler are described in this paper.

1. Introduction

As an upgrade project of Beijing Electron Positron Collider, BEPCII is constructed for two purposes: high energy physics and synchrotron radiation. The designed luminosity of BEPCII is $10^{33}\,cm^{-2}\,s^{-1}$ at 1.89 GeV, which is 100 times higher than that of BEPC. In order to achieve the target luminosity, the beam length is compressed from 50 to 15 mm, while the beam current increases from 70 to 910 mA. Furthermore, two 500 MHz superconducting cavities (SCCs) are used in the BEPCII radio frequency (RF) system instead of four 200 MHz normal conducting as cavities in BEPC [1]. Each superconducting cavity is fed through one high power input coupler. Because of the large beam current, the power delivered through the coupler is very high: 150 kW continuous wave (CW) RF power in traveling wave (TW) mode.

For BEPCII coupler, the main requirements are listed in Table 1 The detailed process including design, fabrication and high power RF conditioning of the coupler is presented in this paper.

2. Design

In the field of superconductivity radio frequency (SRF) of accelerators, the high power input coupler is one of the most critical and complex devices that must perform several tasks simultaneously: (i) transfer RF power from the klystron to SCC and match the impedances of the klystron and the cavity; (ii) serve as an RF-transparent vacuum barrier; (iii) bridge the gap between room and cryogenic temperature and so on [2]. The BEPCII SCC works at 500 MHz, and the input coupler is designed on the basis of the KEKB 508 MHz SCC coupler because of the close operation frequency and its proven excellent performance [3]. The coupler is of coaxial type, which consists of three parts:

1. doorknob to realize the transition from waveguide to coaxial line;
2. RF window to provide RF-transparent vacuum barrier;
3. 50 Ω coaxial line to transfer and feed RF power into cavity.

For the BEPCII coupler, the geometry dimensions have been optimized to match the operation frequency of 500 MHz. The cross-section of the input coupler is shown in Fig. 1.

2.1. Design of doorknob

The doorknob is used to convert the RF power transportation from WR1500 waveguide to 50 Ω coaxial line with good impedance matching. It is composed of a doorknob waveguide and an inner doorknob. The doorknob waveguide connected with WR1500 waveguide is made of aluminum. The inner doorknob is formed by spinning a thin copper plate. Their dimensions shown in Fig. 2 were carefully optimized with respect to impedance matching, peak electric field and some manufacturing issues.

* Corresponding author.
E-mail address: huangtm@ihep.ac.cn (T. Huang).

0168-9002/$ - see front matter © 2010 Elsevier B.V. All rights reserved.
doi:10.1016/j.nima.2010.08.108

Table 1
Main requirements of the coupler.

Requirements	Description
Frequency	500 MHz
Operation power	150 kW with CW
External Q	1.8×10^5
Type	Coaxial, fixed coupling
RF window	Structure: coaxial, planar, with choke structure Dimension: outer, 170 mm; inner 42 mm; thickness 10 mm Material:99.5% Alumina
DC bias	± 2000 V

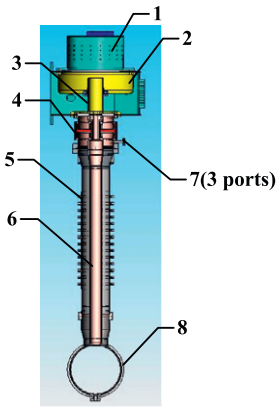

Fig. 1. Input coupler for BEPCII SCC: 1, doorknob cover; 2, doorknob; 3, capacitor to provide DC bias; 4, RF window; 5, outer conductor; 6, inner conductor; 7, monitor ports for vacuum, arc and electron; 8, SC cavity.

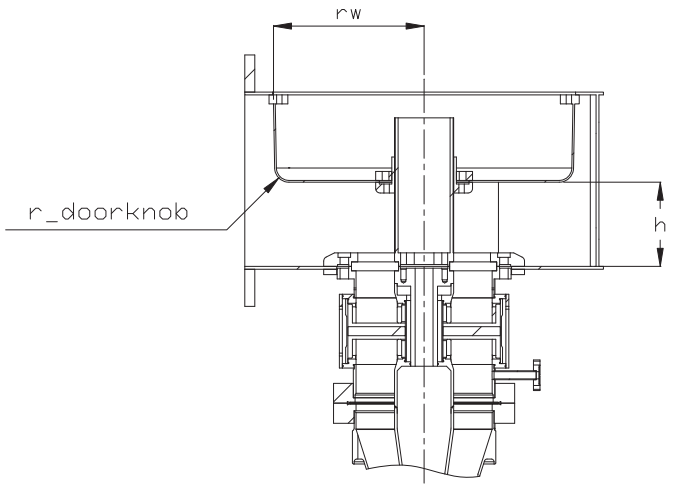

Fig. 2. Three dimensions having important impact on power transmission: 'rw', the diameter of doorknob; 'h', the distance between the doorknob bottom and waveguide; 'r_doorknob', the chamber radius of doorknob.

Among them, the distance between the doorknob bottom and waveguide 'h' has the greatest impact on power transmission. Fig. 3 shows the optimized power transmission performance of the whole coupler structure.

2.2. Design of RF window

A coaxial planar ceramic made of 99.5% alumina has been adopted as the RF-transparent vacuum barrier. Its high dielectric

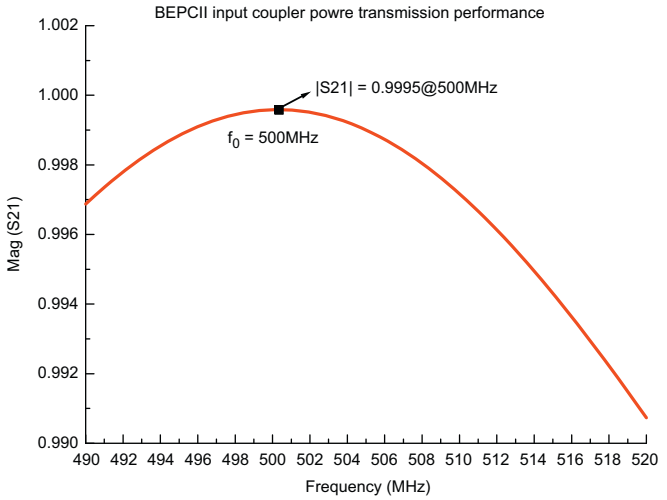

Fig. 3. Magnitude of S21 equals 0.9995 at an operation frequency of 500 MHz as shown in the power transmission curve.

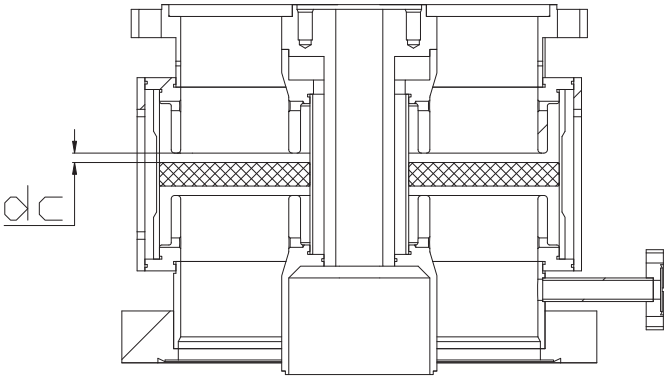

Fig. 4. RF window: both inner and outer conductors have choke structures; a coaxial planar ceramic made of 99.5% alumina has been adopted as RF-transparent vacuum barrier.

constant makes the characteristic impedance of the coaxial line reduced and results in power reflection. An ingenious design that can solve this problem is to increase the diameter of the outer conductor and to decrease that of the inner conductor, that is to say, to form a choke structure (shown in Fig. 4) to keep the impedance constant after introducing the ceramic. Not only the impedance matching is realized, but also the electric field at the window brazing area is decreased. However, the electric field concentrates on the choke tip (shown in Fig. 5), and the electric field on the ceramic surface near the choke tip increases, which may result in local heating and ceramic cracking. A detailed analysis shows that the gap between choke tip and ceramic surface, i.e. 'dc' shown in Fig. 4, plays a critical role on local electric field enhancement. If 'dc' is reduced, the surface electric field will be increased (shown in Fig. 6); on the other hand 'dc' also impacts transmission impedance matching of the coupler. Finally, a compromise was achieved by setting 'dc' as 4 mm.

RF-thermal-structure analysis has been done using ANSYS code. Table2 shows calculated dynamic losses of each part at different power levels. The temperature and thermal stress of RF window are also analyzed. Figs. 7 and 8 show the thermal stress distribution when 300 kW RF power passes through in TW mode without and with 25 °C cooling water on the inner conductor of the window, respectively. It can be seen that the maximum thermal stress with cooling water reduced to 34.9 MPa, which is

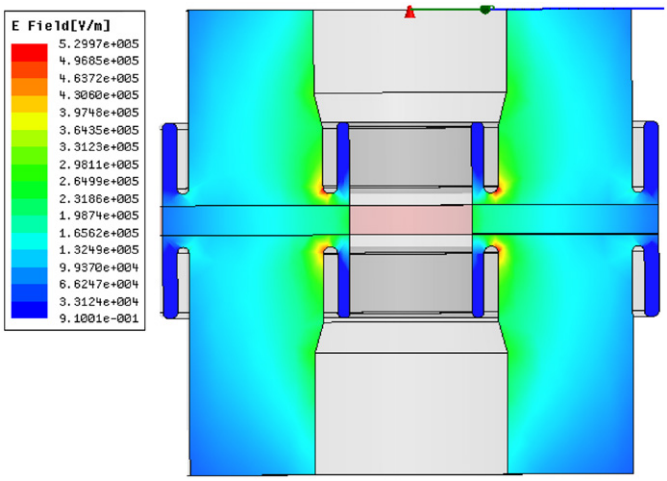

Fig. 5. Simulation of the electric field distribution at RF window with the highest field at the choke tip is shown.

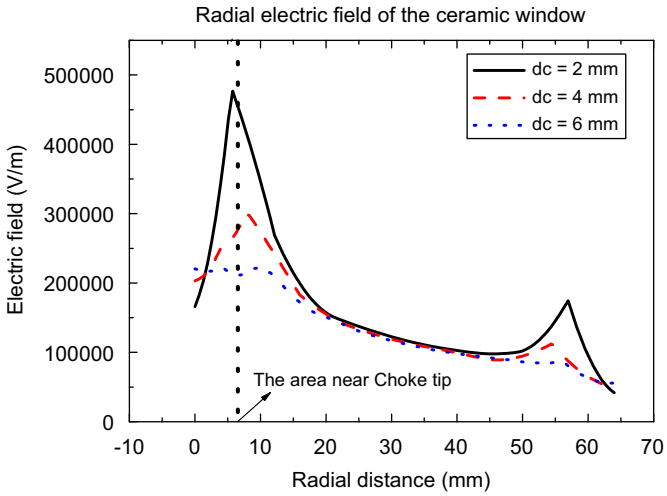

Fig. 6. Radial electric field on ceramic surface decreases with increase in 'dc'.

Table 2
Calculated dynamic losses (W) of every part on different power levels.

Dynamic losses (W)	Pin (kW)					
	50	100	150	200	250	300
RF window	26	52	77	103	129	155
Inner conductor of coaxial line	26	51	77	102	128	153
Outer conductor of coaxial line	11	22	33	45	56	67

only a tenth of the ceramic flexural strength (~330 MPa). The results show that it is enough to use 25 °C cooling water for the inner conductor. The outer conductor of the coaxial line is cooled by 4.2 K helium gas with outside copper fins to obtain a uniform temperature.

2.3. Estimation of external Q

The coupling between cavity and high power input coupler is indicated by external Q usually. The optimized external Q of SCC under heavy beam loading (as shown in Ref. [4]) is

$$Q_{ext} = \frac{V_c^2}{P_b(R_a/Q_0)} \quad (1)$$

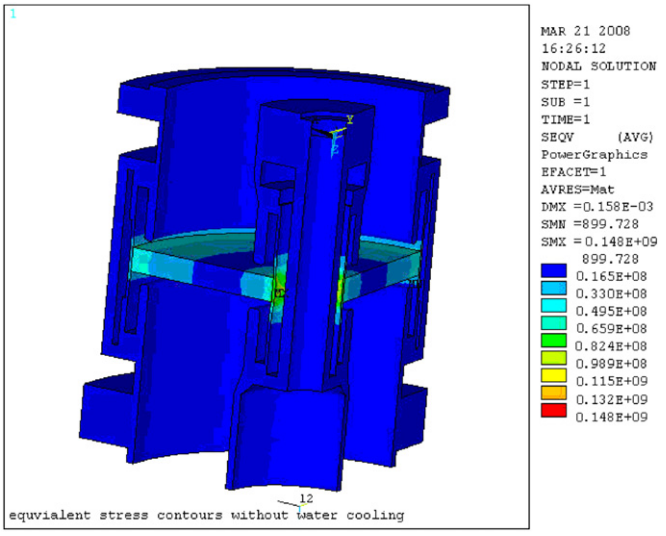

Fig. 7. Simulated thermal stress distribution of RF window while 300 kW RF power passes through in TW mode without water cooling. The maximum stress calculated is 148 MPa at the inner conductor of ceramic.

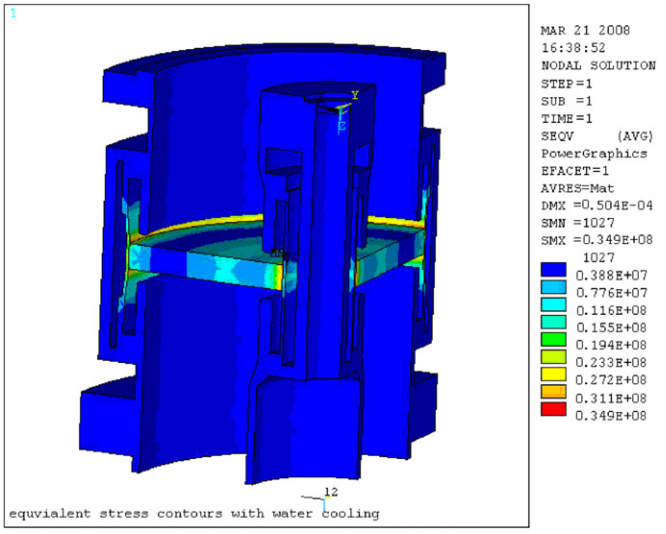

Fig. 8. Simulated thermal stress distribution of RF window while 300 kW RF power passes through in TW mode with 25 °C cooling water on the inner conductor of window. The maximum stress calculated reduced to 34.9 MPa at the inner conductor of ceramic.

where V_c is the cavity voltage, P_b the power transferred to the beam and R_a/Q_0 is a quantity determined by the cavity geometry. For BEPCII SCC, $V_c=1.5$ MV, $P_b=130$ kW, $R_a/Q_0=95.3\ \Omega$ and the optimal Q_{ext} is around1.8×10^5.

Several methods have been developed to calculate the external Q [5]. Here, a time domain method using electromagnetic simulation code is employed to estimate the external Q. This method takes advantage of the built-in waveguide boundary condition, which makes the coupler-cavity system terminated with a matched load. First, the cavity is driven by a Gaussian pulse. Then, a probe is used to record the field energy decaying after the excitation pulse is removed. Through the energy natural decay time constant, the external Q can be calculated directly.

The simulation model is shown in Fig. 9. The beam-pipe lengths on each side of the cavity are chosen to ensure that the fields in the beam pipes will sufficiently evanesce up to the ends

of the geometry, and the length of the coupler coaxial line must be at least half of the wavelength so that the solution of the fundamental transmission line mode has been stabilized. The model solid material is set as vacuum and the boundary as perfect conductor. Fig. 10 shows the energy decay curve as a function of time. The external Q can be calculated from the slope of the energy decay curve K:

$$Q_{ext} = -\frac{10\,\omega_0}{K \ln 10} \tag{2}$$

The four geometry parameters shown in Fig. 11 have been studied [6].Simulation and measured results for various antenna penetration depths have been compared and are shown in Fig. 12. The results have good agreement with an error of less than 10%. Based on the simulation, the corresponding geometry parameters after cooling down are $D=197$, $R_{Tip}=15$, $\Phi\_SBP=220$ mm and the antenna penetration depth into the beam-pipe is about 2 mm. Considering the thermal shrinking from room temperature to liquid helium temperature, the antenna penetration depth in normal temperature can be determined.

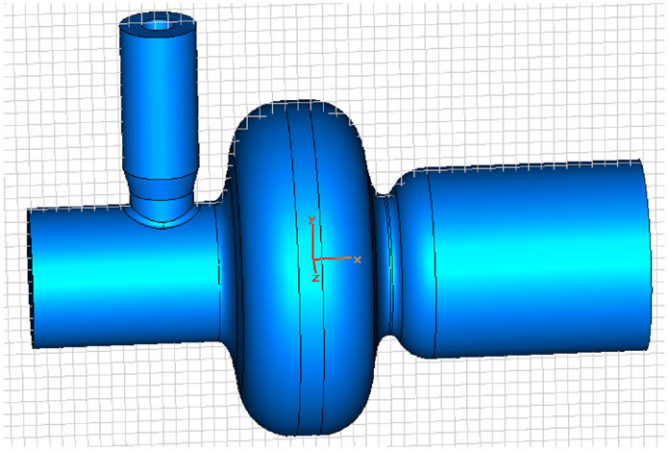

Fig. 9. Simulation model: the length of the beam-pipes and coupler coaxial line should be long enough to assure an accurate simulation.

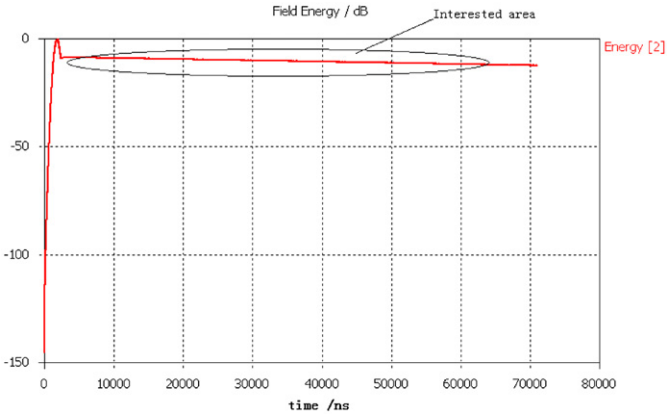

Fig. 10. Energy decay curve as a function of time: the external Q can be calculated from the slope of the energy decay curve K.

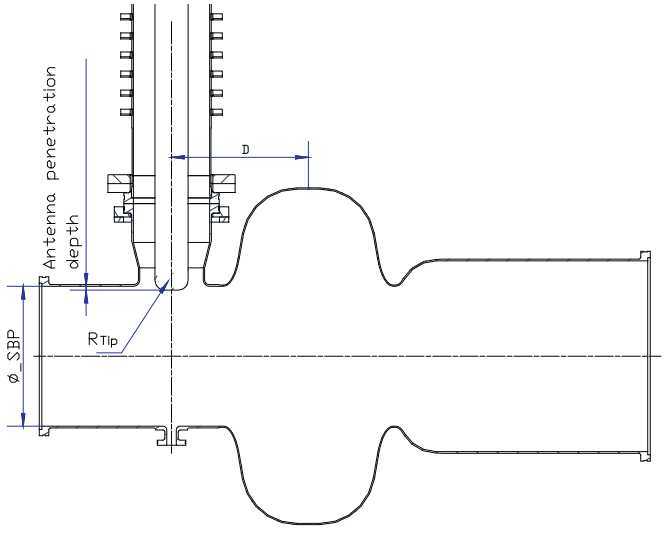

Fig. 11. Four dimensions have important impact on coupling: (1) antenna penetration depth; (2) R_{Tip}, antenna tip radius; (3) Φ_SBP, small beam pipe diameter; and (4) D, distance between the coupler axis and the cavity equator perpendicular bisector.

3. Fabrication [7]

After careful RF, thermal and structure analysis, the whole coupler structure was determined. Then, we started the fabrication of prototypes. The fabrication started with the machining of 112 individual parts. Then, all parts were degreased and deoxidized carefully according to the clean requirements of ultrahigh vacuum and high power operation. After that, a series of processes such as welding, copper plating and TiN coating were carried out for sub-assembly construction. Finally, a whole

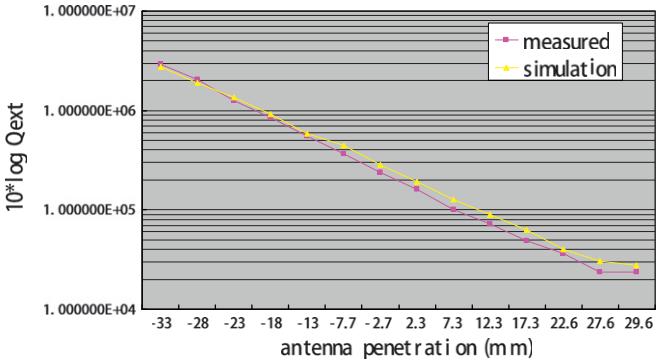

Fig. 12. Simulated and measured external Q for various antenna penetration depths that have good agreement with an error of less than 10%.

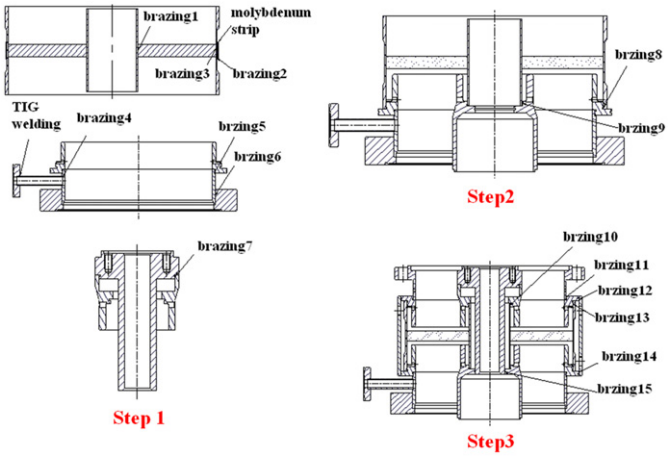

Fig. 13. Three steps involved in the RF window brazing.

coupler is assembled, leak checked and cleaned in a class 100 cleaning room. The fabrication of some key components proved particularly challenging.

3.1. RF window brazing

The RF window is made up of 20 parts. The large diameter and high purity (42 mm × 170 mm × 10 mm, 99.5% alumina ceramic) made the brazing between the ceramic and the solid copper very difficult. Also, the complicated choke structure increases the brazing difficulty. The three steps shown in Fig. 13 were involved in RF window brazing. The first brazing was carried out at about 1000 °C by AuCu(Cu65%). Then the following brazing was processed at about 900 °C by AuCu(Cu20%) and the last brazing was carried out at about 800 °C by AgCu(Cu28%). After several technical experiments, a series of methods were developed to improve brazing, such as making the outer conductor tied with molybdenum strip to restrain thermal expansion, selecting and arranging the solder wires carefully to improve solder creeping and optimizing the temperature increment speed to keep the brazed parts heated uniformly. Window brazing was processed in vacuum furnace to protect the TiN film coated on the vacuum side of ceramic from damage.

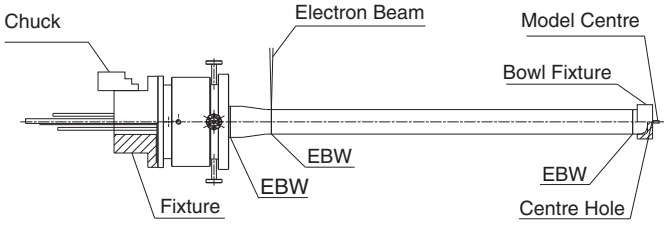

Fig. 14. A chuck and a bowl-shaped fixture with a centre hole were designed to keep the concentricity of the long antenna during EBW.

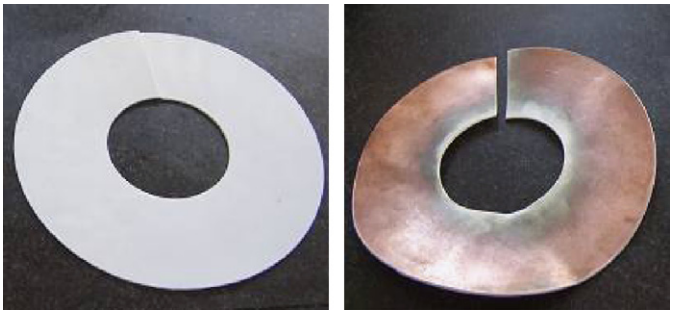

Fig. 15. Ceramic shield before (left) and after (right) EBW: a large amount of copper vapor spattered and condensed on the Teflon.

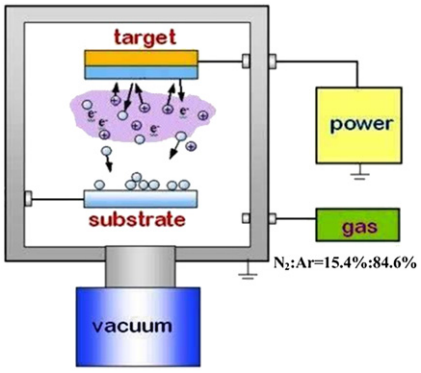

Fig. 16. TiN coating mechanism: a normal DC spattering was used.

3.2. Antenna welding

For antenna welding, the main challenges are described as follows: (1) how to keep accurate concentricity of the antenna long up to 1.4 m after welding; (2) how to satisfy a fine surface finish of welds and (3) how to protect ceramic surface from contamination. Electron beam welding (EBW) proved to be the best choice in the end. A bowl-shaped fixture with a centre hole was designed to keep the concentricity of the long antenna (see Fig. 14). Meanwhile, a piece of TeflonR shown in Fig. 15 was used to protect the ceramic. We find that a large amount of copper vapor spattered and condensed on the Teflon.

3.3. Outer conductor copper plating

The outer conductor was made of stainless steel for high mechanical strength and low static heat leak to SCC. However, its inner surface should be copper plated to minimize RF losses. The thickness of the copper plating layer was designed considering both RF losses and static heat leak. After thermal analysis with ANSYS code, the optimized thickness is about 30 μm. The major difficulty was how to obtain good uniformity, high adhesiveness and free of bubbles copper plating layer. After some trial-fail experiments, we found that optimizing the current value according to the size of the plated parts was very effective to obtain a fine plating layer. After plating, the plated parts should be heated in a hydrogen furnace with a temperature up to 500 °C, which can not only identify but also improve the adhesiveness and electrical conductivity of the plating layer [8].

3.4. Ceramic TiN coating

Since the secondary emission coefficient of the Al_2O_3 ceramic is high, while that of TiN is less than unity over a wider range of impact energy [9], the vacuum side of ceramic is usually TiN coated to avoid multipacting. Through experimental research, we find that the desired thickness of the TiN film is about 80 Å. The difficulty encountered was how to control the thickness and uniformity of the coating layer accurately. Fig. 16 shows the TiN coating mechanism. A normal DC spattering was used. A plate shape Ti target acted as anode and the outer conductor of the window as the cathode. High voltage up to 2 kV was added between the anode and the cathode. The nitrogen–argon mixed gas (nitrogen:argon = 15.4%:84.6%) was ionized by the high voltage field and the accelerated ion bombarded the Ti target. In the end, Ti^+ and N^- generated TiN, which was deposited on the surface of the ceramic. The thickness of TiN film is controlled by the spattering time. The ceramic coated has a high resistance up to 2000 MΩ.

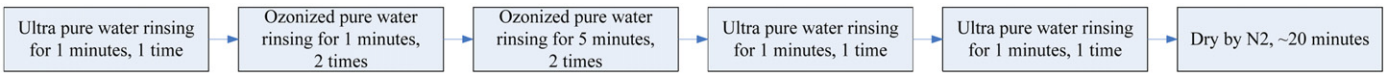

Fig. 17. Cleaning procedure.

4. High power RF conditioning

For high power input couplers, high power RF conditioning is necessary. There are two purposes: one is to test the coupler performances to check whether they satisfy design requirements or not; and the other is to make the coupler operate well at nominal power levels by removing residual gases, dust and particles in the RF conditioning.

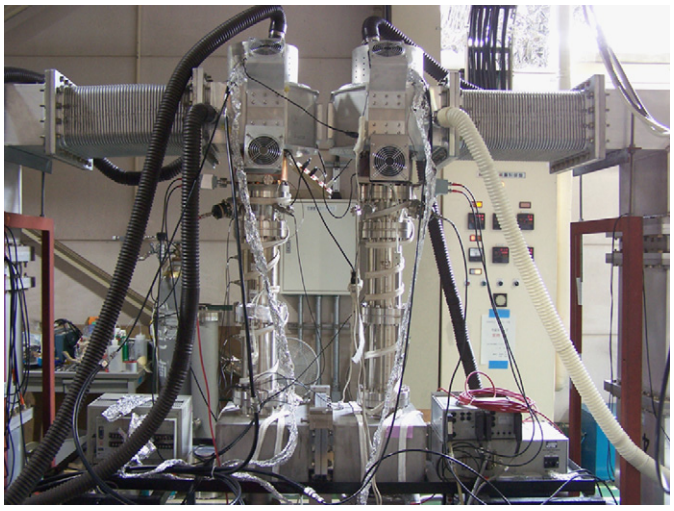

Fig. 18. Test stand consists of a pair of back to back couplers, one connected waveguide, vacuum system and monitoring system.

4.1. Preparation

In the first step, all components of the input couplers were cleaned carefully in a class 100 clean room. Fig. 17 shows the detailed cleaning procedure.

After cleaning, the coupler was assembled onto a test stand quickly in class 1000 clean room. The test stand consists of a pair of back-to-back couplers, one connected waveguide, vacuum system and monitoring system, as shown in Fig. 18. RF power is transmitted from the upstream test coupler, through the connected waveguide to the downstream referent coupler and then to a water-cooled terminating load or to a variable short circuit. The vacuum system includes two turbo-molecular pumps of 50 L/s and one ion pump of 100 L/s. An arc sensor is attached near the window and a view port is added at the bottom side of the connected waveguide to detect discharging. A vacuum gauge is located near the window to observe outgasing and to realize vacuum interlock control further. Eight electron probes are equipped on the outer conductor to identify multipacting positions and intensity. Several thermocouples are placed on the doorknob and the outer conductor to measure the temperature.

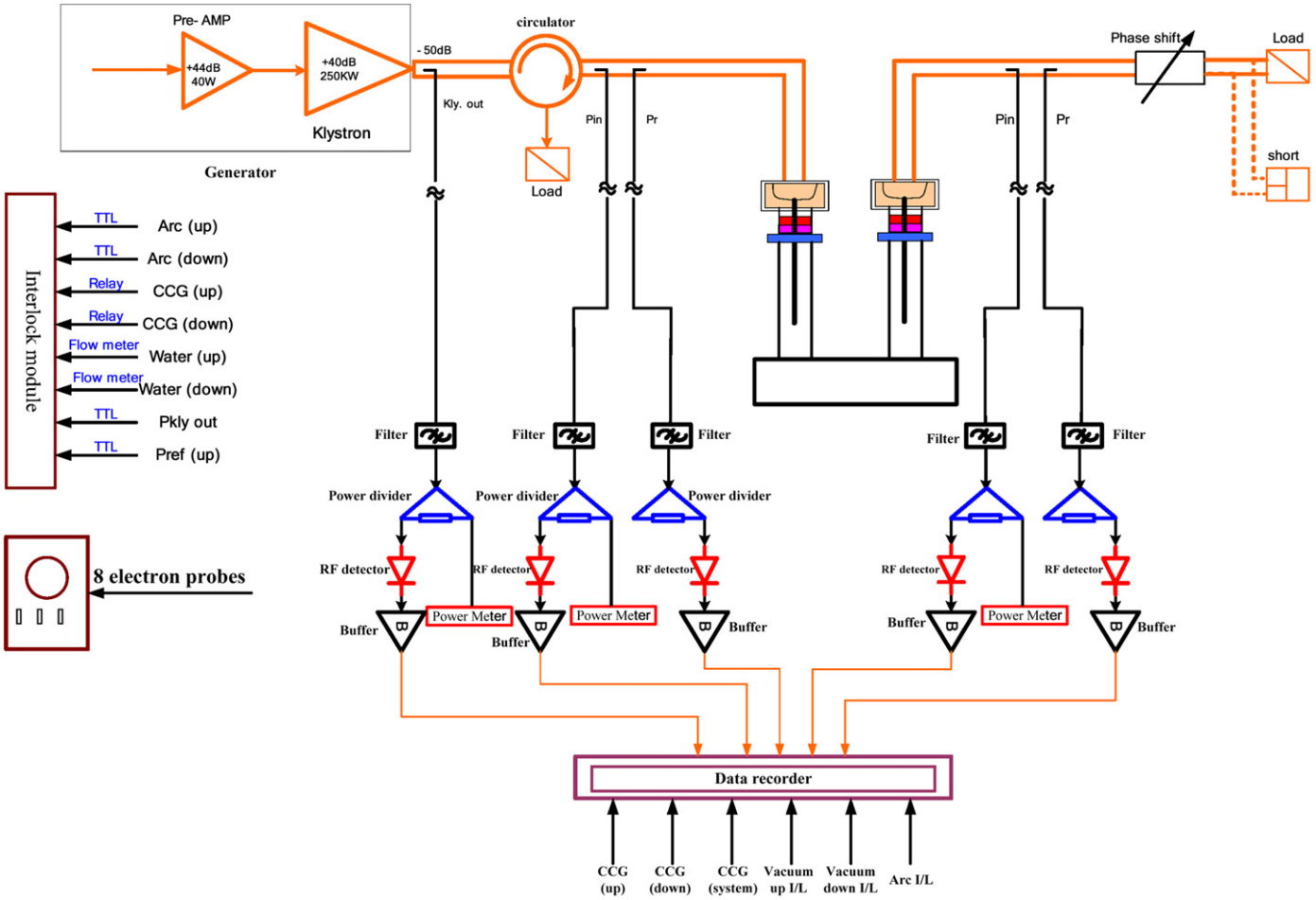

Fig. 19. Low level RF interlock control system: it consists of interlock module, power control module, power meter and data recorder and so on. There are eight interlock signal: 1: arc (up), discharge near upstream coupler window; 2: arc (down), discharge near downstream coupler window; 3: CCG (up), vacuum pressure near upstream coupler window; 4: CCG (down), vacuum pressure near downstream coupler window; 5: water (up), cooling water for upstream coupler; 6: water (down), cooling water for downstream coupler; 7:Pkly out, forward RF power from generator; and 8: Pref (up), reflection RF power before upstream coupler.

Then, the whole test stand was baked at 150 °C for 24 h. First, this operation reduces the water level in the coupler, which will fasten RF conditioning. Actually, by our experiment result, a proper increase in baking time is very useful to save conditioning time. Second, it checks any dilatation effects, mechanical constraints and weld quality of the key components. Many defects have been discovered at this stage actually, avoiding serious problems later.

4.2. High power RF conditioning

RF conditioning increases the power through the input coupler step by step under strict control of discharging and outgasing and reach the required operation power condition in the end. Fig. 19 shows the low level RF interlock control system. It consists of interlock module, power control module, power meter and data recorder and so on. Eight interlock signals such as discharge, vacuum, forward and reflection power and so on are monitored all the time to prevent a fatal discharge near the ceramic window. Electron currents extracted by eight electron probes on outer conductors were read by an oscilloscope.

Initially, a conventional method with only CW RF power increasing gradually was applied. However, many serious discharging and outgasing occurred at the low power level, especially between 30 and 45 kW, which can be proved from the number of monitoring sensor-initiated triggers shown in Fig. 20. Then a new conditioning method was developed to obtain a compromise between conditioning speed and discharging risk. The process of the new conditioning method is shown in Fig. 21. First, pulse conditioning was adopted. During the pulse conditioning, the

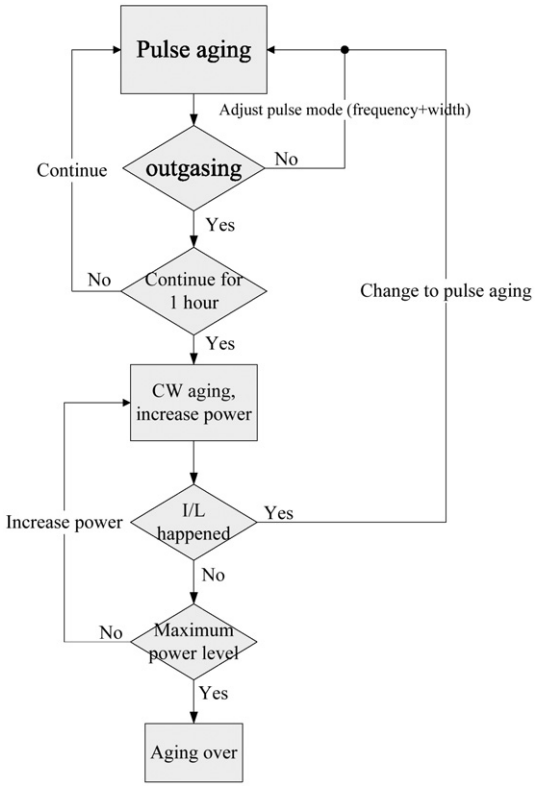

Fig. 21. Process flow of new conditioning method: pulse-continuous-pulse conditioning repeatedly instead of conventional only CW conditioning.

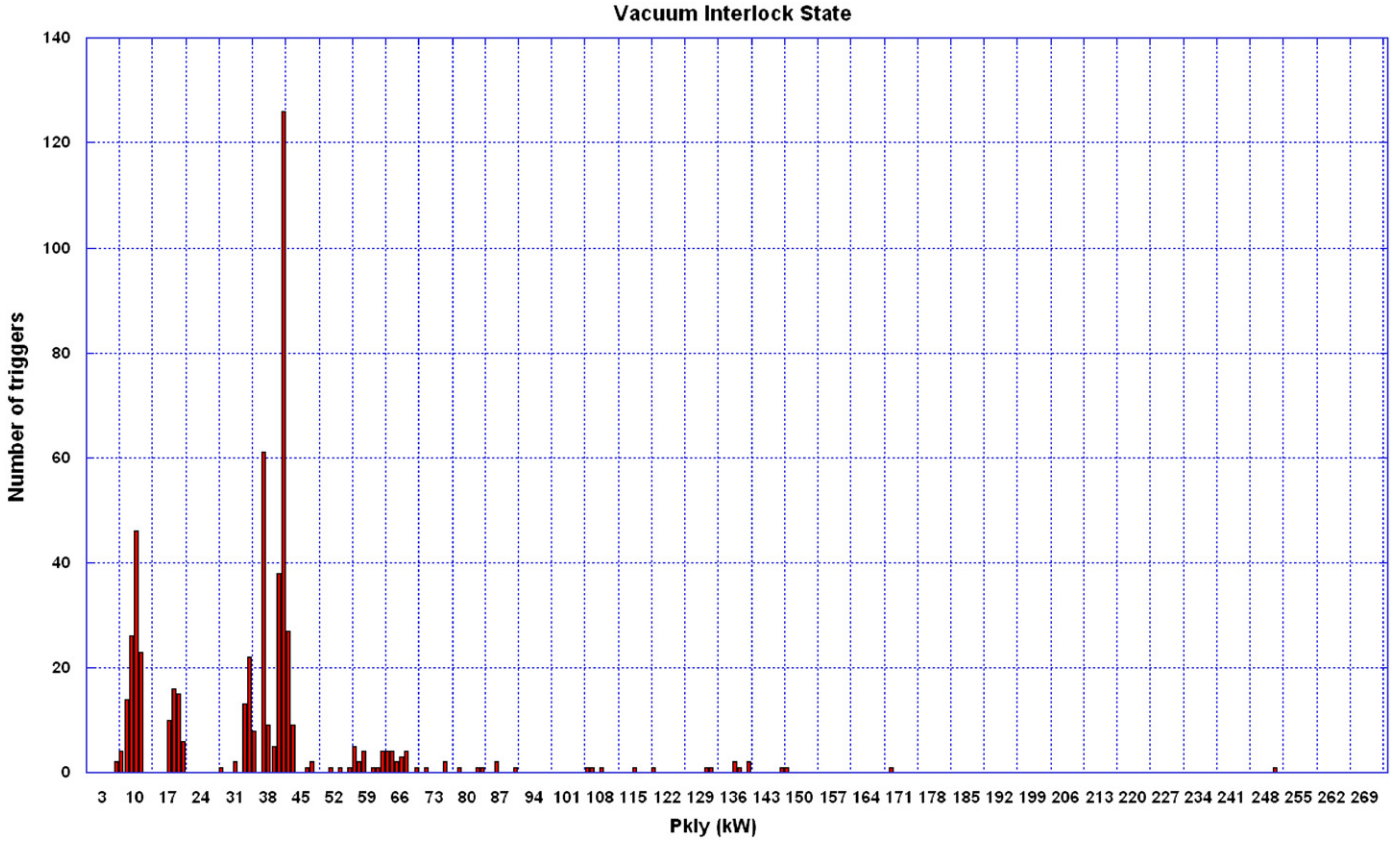

Fig. 20. Number of monitoring sensor-initiated triggers are more than 120 between 30 and 45 kW, while it reduces obviously after the new method applied above 50 kW.

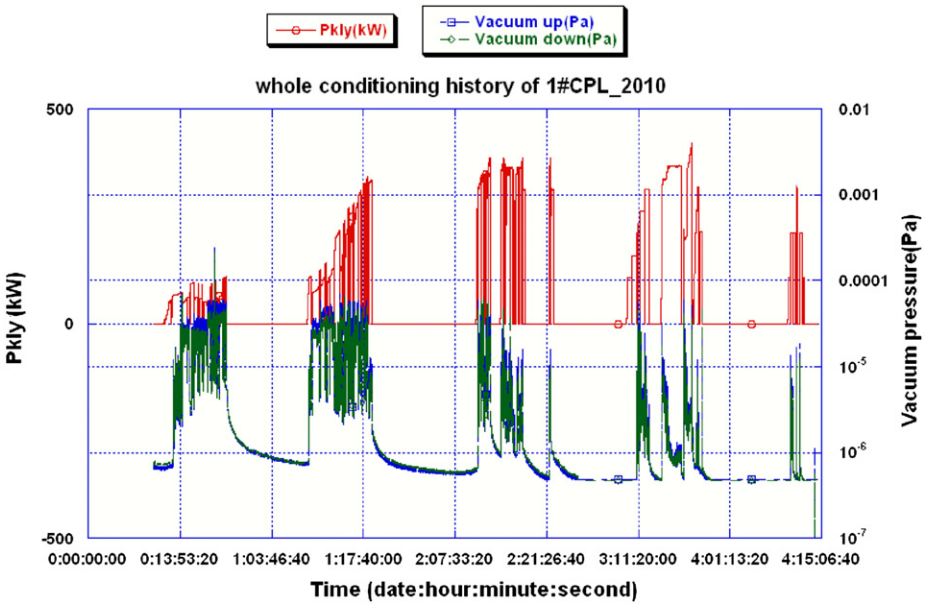

Fig. 22. Maximum power of 420 kW was reached for 1#CPL_2010 after 40 h conditioning: forward RF power from generator (upside), vacuum pressures near the RF window of upstream test coupler and downstream reference coupler (downside).

pulse amplitude, width and repetition rate were adjusted continuously to keep outgasing, discharging and electron current intensities around the interlock levels. About 1 h later, continuous wave was used to check the pulse conditioning effect. Once discharging or outgasing is finished, switch to pulse conditioning. The conditioning process of pulse-continuous-pulse was repeated until nominal power levels were reached. This method proved very effective. As can be seen from Fig. 20, the number of triggers reduces obviously after the new method applied above 50 kW. That is because the desorption gas has been removed rapidly before outgasing and discharging interlock triggered with short pulses and sufficient rest time. Another effective method of reducing conditioning time is to increase vacuum interlock threshold value gradually as the intensity of electron and discharge decreases. In our case, the vacuum pressure near RF window of both upstream coupler and downstream coupler were monitored carefully. The threshold value was changed from 5E−5 to 8E−5 Pa, which proved safe and effective for conditioning.

Four couplers have been tested by CW RF power on IHEP test stand and KEK test stand. During the test, each coupler to be tested was connected with one reference coupler in the way shown in Fig. 18. Here, the reference coupler is a coupler having been tested and proved exceeding RF performance. 1#CPL_2008 reached more than 270 kW in 2008 and 2#CPL_2010 reached over 300 kW in 2010, especially, a maximum power of 420 kW was reached for 1#CPL_2010 after 40 h conditioning. 3#CPL_2008 was tested in IHEP and a CW RF power of 180 kW was achieved. Fig. 22 shows the whole conditioning history of 1#CPL_2010.

5. Conclusion

A high power input coupler for BEPCII 500 MHz SCC has been developed in China. The coupler structure has been designed carefully from the view of impedance matching, electric–magnetic and thermal stress optimization. The external Q was calculated to determine the coupling port dimensions. Several prototypes were successfully fabricated and tested. Whole fabrication procedure and key technologies based on Chinese industry have been developed, such as copper plating, window brazing, EBW and TiN coating. A maximum of 420 kW CW RF power in TW mode has been reached after 40 h conditioning in April 2010, which can satisfy BEPCII requirement well.

Acknowledgements

The authors would like to thank Hai-ying Lin, Guang-yuan Zhao, Xiao-hua Peng, Qi-wang Wang, Kun-peng Li and Xiu-xia Li for their excellent technical support during coupler fabrications and high power tests.

They have benefited from many discussions with high power input coupler people, W.-D. Moller, T. Kijima and E. Montesinos.

References

[1] Zhongquan Li, Chuang Zhang, High Energy Physics and Nuclear Physics 27 (10) (2003) 919.
[2] Wolf-Dietrich Moeller. High power input couplers for superconducting cavities, in: Proceedings of SRF2007, Beijing, China, 2007.
[3] Y..Kijima, S..Mitsunobu, T..Furuya, et al. Input coupler of superconducting cavity for KEKB, in: Proceedings of EPAC2000, Vienna, Austria.
[4] Hasan Padamsee, Jens Knobloch, Tom Hays, in: RF Superconductivity for Accelerators, John Wiley & Sons, Inc., New York, 1998, pp. 381-389.
[5] Derun Li, Robert Rimmer, Shakti Kosta. Calculations of external coupling to a single cell RF cavity, in: Proceedings of the LINAC Conference 1998, p. 977.
[6] H.U.A.N.G. Tongming, P.A.N. Weimin, et al., Chinese Physics C 32 (01) (2008) 72.
[7] H.U.A.N.G. Tongming, M.A. Qiang, P.A.N. Weimin, et al., Chinese Physics C 32 (11) (2008) 931.
[8] Wolf-Dietric Moeller. fabrication issues on the high power couplers for TTF, in: Proceedings of the ERL-mini Workshop, Beijing, China, 2005.
[9] F.L..Krawczyk. Status of multipacting simulation capabilities for SCRF applications, in: Proceedings of the 10th Workshop on RF Superconductivity, Tsukuba, Japan, 2001.